Ocean-atmosphere coupling in the Mediterranean Sea from TOPEX/POSEIDON, ERS1 and AVHRR data

Elisa Garcia-Gorriz , Jorge Vazquez-Cuervo

Jet Propulsion Laboratory/California Institute of Technology, Pasadena, California, USA

Corresponding author address: E. Garcia-Gorriz, JPL/ Caltech, MS 300/323, 4800 Oak Grove Dr., Pasadena, California 91109 (USA). E-mail: eg@pacific.jpl.nasa.gov

Abstract

The objective of this work is to evaluate the patterns of the ocean-atmosphere coupling in the Mediterranean sea using the statistical analysis of the time series of three satellite measured variables: wind stress curl computed from the surface wind velocities measured by the European Remote Sensing Satellite- ERS1, sea level anomalies from the merged ERS1-TOPEX/POSEIDON altimetric data and the sea surface temperature from the NOAA/NASA Pathfinder AVHRR Oceans Project. This study examines the ocean-atmosphere coupling patterns in time and space through a canonical correlation analysis of the fields. The wide and exhaustive coverage of the oceanic and atmospheric fields from satellites (such as TOPEX/POSEIDON and ERS1) allow a potential detailed inspection of the coupling. In this study assess the role of wind stress and/or sea surface temperature space/time variations as forcing mechanisms of the sea level variability for the total 440 day duration (from October 1992 to December 1993) of the three satellite data sets in the different Mediterranean sub-basins. The linear barotropic vorticity equation is computed in order to estimate if the Mediterranean sea level response to wind forcing is barotropic. Results indicate that except for the Strait of Sicily and the Adriatic sea the barotropic response is not dominant. From the canonical correlation analysis, a correlation of 0.57 for the first mode between the sea level anomaly and the wind stress curl indicates a significant local coupling between them, especially in areas of the Eastern Mediterranean. Two uncoupled annual cycles are found in the sea surface temperature data.

seasonal

1. Introduction

The Mediterranean sea is a midlatitude semi-enclosed sea connected to the Atlantic Ocean by the Strait of Gibraltar and to the Black sea by the Dardanelles/ Bosphorus straits. It is divided into two main basins: the Western and the Eastern Mediterranean (named hereinafter WM and EM, respectively). The WM and EM are connected by the Strait of Sicily (see Fig. 1a). Both the WM and EM are divided into smaller sub-basins, each of which with its own characteristic circulation and dynamics (see Roussenov et al., 1995, figure 1 for a schematic of surface circulation features in the Mediterranean sub-basins; the Algerian current is schematicly located with a dashed-line rectangle in Fig. 1a). From west to east, the Alboran, Catalan, Balearic, Ligurian and Thyrrenian sub-basins constitute the WM, while the Ionian, Adriatic, Aegean and Levantine sub-basins make up the EM.

The inflow of Atlantic water (and outflow of Mediterranean water) through the Strait of Gibraltar and the thermohaline forcing, along with the wind stress curl, and bathymetry are considered the principal factors governing the general circulation patterns in the Mediterranean sea. The Mediterranean circulation is chiefly thermohaline (Font, 1987): its waters are mainly driven by the net fresh water loss and heat loss to the atmosphere and the exchange of salinity and heat through the Strait of Gibraltar (inflowing Atlantic water vs. outflowing Mediterranean water). The loss through evaporation exceeds the precipitation plus river runoff and Black sea exchange (Zavatarelli and Mellor, 1995). In the Mediterranean surface layer, the Modified Atlantic Water is subject to evaporation and mixing with the underlying waters, causing a progressive downstream increase of salinity. The Mediterranean outflow consists primarily of Levantine Intermediate Water (result of the EM winter convection processes) which reaches the Strait of Gibraltar, along with the WM Deep Water which is produced in the Gulf of Lions area (Zavatarelli and Mellor, 1995). As Malanotte-Rizzoli and Bergamasco (1991) pointed out by means of numerical experiments, the wind stress and the air-sea thermal fluxes are also fundamental driving mechanisms that govern the circulation, especially in the EM. The transport through the Strait of Gibraltar constitutes one of the major forcing mechanisms of the circulation of the WM and is responsible for the basin-scale cyclonic flow (Millot, 1987).

The objective of this paper is to evaluate the coupling between the ocean and the atmosphere from the statistical analysis of the time series of three variables: wind stress curl (hereinafter referred to as WSC) computed from the surface wind velocities provided by the

European Remote Sensing Satellite (ERS1), sea level anomaly (hereinafter named SLA) from the merged ERS1 - TOPEX/POSEIDON altimetric data and the sea surface temperature (hereinafter named SST) from the NOAA/NASA Pathfinder Advanced Very High Resolution Radiometer (AVHRR) Oceans Project. This study examines the ocean-atmosphere coupling patterns in time and space through a statistical comparison of the fields. The wide and exhaustive coverage of the oceanic and atmospheric fields from satellites (such as TOPEX/POSEIDON and ERS1) allow a potential detailed inspection of the coupling.

In general, sea level varies temporally due to many causes, including fluctuations in atmospheric pressure, wind stress, solar heating and cooling, fresh water fluxes, and tides. This also occurs in the Mediterranean sea. Wunsch (1972) examined the complete physics of sea level fluctuations from periods within 2 hours to 8 years and demonstrated that although sea level variability is dominated by tides and atmospheric pressure loading, it is significantly coherent with changes in the Ekman pumping from the fluctuating local WSC. For this reason WSC is used instead of wind velocity in this study. Additionally, Gill and Niiler (1973) concluded that the seasonal variations in sea level are dominated in midlatitudes by expansion and contraction of the water column above the thermocline caused by the seasonal surface heating and cooling, and surface fluxes of water. By evaluating the coupling between the ocean and the atmosphere we intend to assess the role of WSC and/or SST space/time variations as forcing mechanisms in producing SLA variability for the 440 day duration of the overlap of the three data sets in the different Mediterranean sub-basins (from October 7 1992 to December 11 1993). Using merged ERS1-TOPEX/POSEIDON altimetric data improves the spatial resolution of the TOPEX/POSEIDON alone and enables the resolution of mesoscale structures which are significant in the Mediterranean circulation (LeTraon et al., 1995).

It is known that a significant correlation exists between winds blowing southward in winter and intensive sea surface cooling in some areas of the Mediterranean sea. This winter situation occurs in the Gulf of Lions and concurs with deep water formation processes (Leaman and Schott, 1991). Thus, an issue is the potential correlation between the WSC and SST for the entire Mediterranean sea within the time span of this study. On the other hand, Larnicol et al. (1995) concluded from the visual comparison of plots of WSC and SLA rms in the Mediterranean that there are coincident maxima and thus winds can be expected to play an important role in forcing the circulation.

The paper is organized as follows. Section 2 has a description of the data sets and the processing analysis performed on the data. Section 3 (a) describes the analysis focusing on the frequency spectra of the three data sets. Section 3 (b) discusses the application of canonical correlation techniques (Kelly et al., 1996) to the SLA, WSC and SST and the dynamical information resulting from the canonical modes. Section 3 (c) focuses on the results from the computation of the linear barotropic vorticity equation for WSC and SLA in order to assess the barotropic response of the Mediterranean sea. The response of the ocean to wind forcing is considered to be primarily barotropic at mid and high latitudes when the scale of the forcing is larger than 100 km and the period of the forcing is between the inertial period and about 300 days (Fu and Davidson, 1995). Such assumptions are applicable to our time/space ranges in the Mediterranean sea. Section 4 has the summary and conclusions.

2. Data and Methodology description

Forty-four consecutive maps of the SLA have been produced by merging and interpolating ERS1 and TOPEX/POSEIDON altimetric data onto a regular 0.2 degree grid resolution in latitude and longitude over the Mediterranean sea via objective analysis (LeTraon et al., 1995). The time step between consecutive maps is 10 days; these maps have a 150 km spatial correlation scale. For both ERS1 and TOPEX/POSEIDON data sets the usual environmental corrections have been applied: inverse barometer, tides, electromagnetic bias, ionospheric, and wet and dry tropospheric corrections (Ayoub et al., personal communication). The spatial and temporal resolution is increased by merging the TOPEX/POSEIDON and ERS1. Figure 1(b) shows the ground track locations for both ERS1 (thin lines) and TOPEX/POSEIDON (thick lines) over the study area.

The orbit errors for ERS1 were reduced by using TOPEX/POSEIDON data as a reference. The orbit accuracy of this merged altimetric data set is of the order of 3 - 5 cm (for further details on ERS1 orbit correction see LeTraon et al., 1995). The period of study corresponds to cycles 6 to 18 for ERS1 and cycles 2 to 49 for TOPEX/POSEIDON, beginning in October 1992 and ending in December 1993. For both data sets, the SLAs have been computed by removing the one year mean from December 1992 to December 1993 (Ayoub et al., personal communication).

The WSC is computed from ERS1 scatterometer wind velocity gridded data. The spatial

resolution of the wind velocity data is 1 degree and they are sampled every 12 hours. First, the wind velocity vector at 10 meters was converted to wind stress by using $\tau = \rho_a C_d |V| V$, where ρ_a is the density of air at the surface (assumed constant), Cd is the empirical drag coefficient, and V is the wind vector adjusted to 10 meters above the sea surface. The value used for Cd fulfills the following equation (Smith, 1980): $Cd = 0.61 + 0.063\,|V|$ (1)

The WSC was computed afterwards using a finite difference scheme over a spatial resolution of 1 degree. To approximate the e-folding time scale of the SLA interpolation the WSC was low-pass filtered, removing periods shorter than 15 days. These values were averaged over 10 days and then spatially interpolated to 5 points per degree using a bilinear interpolation over the same SLA spatial grid points.

The SST data used in this study corresponds to version 4 of the SST data from the NOAA/NASA AVHRR Oceans Pathfinder Project. The SST daily maps have a spatial resolution of 9.28 km. The SST data set was also averaged over 10 days and spatially interpolated over the same SLA and WSC time/space grid points. Using only the cloud-free pixels in the SST maps, a bilinear interpolation over a 40 km spatial radius of influence was applied over those pixels identified as clouds, thus filling in spatial gaps in the data. This scheme was successful because ninety percent of all possible pixels from October 1992 to December 1993 were found to be cloud free.

For the SLA, WSC and SST data sets, an analysis of the frequency spectra indicates a dominant annual signal is present. Thus to study the non-annual (or filtered) response, the annual cycle was removed through the fitting of an annual harmonic. The canonical correlation modes for WSC, SLA and SST and the linear barotropic vorticity equation are computed using the filtered data sets with the annual signal removed.

3. Results and discussion

a. The annual signal coupling

To examine the energy in the frequency spectra of the SLA, SST and WSC, the power spectral density at each grid location was calculated via the Fast Fourier Transform (FFT). A spatial ensemble average was then calculated over all the grid locations in the Mediterranean. The three plots of the power spectral density in Fig. 2 show the dominance of the annual cycle. The seasonal signal seems to be much stronger in the Mediterranean sea than in other parts of the

world ocean (Malanotte-Rizzoli and Bergamasco, 1989). Fig. 2a indicates that for the SLA there are two local maxima, at about 3 and 7 cycles per year, while for the SST (Fig. 2b) there is one at about 4. For the WSC, peaks in the spectrum are observed at about 4 and 7 cycles per year. No significant peaks occur at the semiannual period. This fact could mean that the semiannual frequency has about the same relative energy associated with it as other non-annual frequencies. This will be discussed later in the paper in the context of the temporal part of the canonical modes.

We extracted the dominant annual signal from the three data sets in the Mediterranean by removing an annual harmonic fit to the data. Figure 3a,b,c display the spatial average of the annual signal for the WM and EM respectively. In both basins there is a direct correlation between the spatial structures of the annual signal of SLA and SST. The SLA and SST maxima are coincident for the WM at day 641 (October), but with a 5 day lag in the EM: 656 for SLA and 651 for SST (both October). Our results are consistent with Larnicol et al. (1995) when they computed the time variation of the spatially averaged sea level in the Mediterranean, which is related to the thermal forcing in the Mediterranean. They concluded that the mean observed variation and thermal forcing were in phase and that the latter only appeared to account for a portion of the observed variation from the mean sea level.

Our results correspond to the basin-wide average having removed the contribution of the Adriatic sea. The annual signal in the Adriatic sea behaves differently with respect to the EM and reaches a maximum at day 631 and a minimum at 451. The Adriatic sea is decoupled with respect to the rest of the EM, most likely due to its shallow depth and characteristic wind forcing regime. The variability of the basin-wide thermal pattern in the Adriatic reveals a seasonal response (four distinct seasons), which is different from both the EM and WM, where only two major patterns are recognized (Gacic et al., 1997).

The lag between the EM and WM for the SLA and SST is of several days, as observed in Fig. 3a and c respectively. The WM reaches earlier maximum values for SLA and SST but these maximum values are lower than the maxima within the EM. For the SST this result can be caused by the effect of the latitudinal variation of insolation, as the EM is more southern than the WM, and also by the cooler Atlantic water inflow through the Strait of Gibraltar in the WM.

The annual signal of the WSC (Fig. 3b), behaves such that the maxima are at day 361 (December) for the WM and day 401 for the EM (February). Therefore, there is a lag of several

days in the annual signal between WM and EM for the three data sets. In all three data sets, maxima and minima are reached earlier in the WM than in the EM and the amplitudes of the annual signals are less in the WM than in the EM. With the mean values removed, the ranges are shown in Table 1.

The amplitudes of the annual signals are shown in Fig. 4a,b,c for SLA, WSC and SST respectively. For the SLA, the maximum amplitudes are larger than 15 cm and they are located in the Alboran and Levantine sea (Fig. 4a). Large amplitudes are accompanied by high values corresponding to the WSC annual amplitude in the Ionian and Levantine sea (Fig. 4b). Southeast of Crete there is a coincident maximum for both WSC and SLA. It is also observed in the amplitude of the filtered (annual cycle removed) SLA (Fig. 6a). This maximum variability in sea level anomaly in this area is associated with a maximum in geostrophic velocity (Larnicol et al., 1995) and this maximum value for both WSC and SLA corresponds to a gyre-structure due to the sheltering effect of the island of Crete. This could be identified with the Ierapetra gyre (Larnicol et al., 1995), although it does not appear in the SST field. For the SLA, the annual signal explains a large percentage of the variability for the entire Mediterranean sea, while the WSC in the Ionian (with a patch in the southern Thyrrenean sea) and Levantine sea have higher values in terms of the percent variability explained by the annual signal in the Mediterranean. Both the northwest region of the WM (two patches east and west the Gulf of Lions) and the central region of the Algerian current have maxima in the WSC annual signal associated with minima in the SLA. The Algerian current has a local maximum in variability: most likely due to its instabilities and generation of mesoscale eddies (Bouzinac et al., 1998).

The percent of variability explained by the annual signal for SST (30-40%) is lower than SLA and uniform for the whole Mediterranean sea. Except for the Adriatic, the distribution of the SST amplitude in Fig. 4c can be described latitudinally: the higher annual amplitude (13 °C) are located in the most southern basins (Ionian and Levantine) and the Thyrrenian sea, which are also the furthest basins from the Strait of Gibraltar. This latitudinal distribution can be associated with the synoptic seasonal warming. The spatial plot of the annual signal for SST in the Alboran sea reflects the cooler Atlantic inflow as well as it captures the energetic double-gyre pattern of slightly warm water in the Alboran sea surface. In addition, the northern-most WM (including the areas of the Ligurian sea, Gulf of Lions and Northern Catalan sea) show lower SST annual amplitudes (7 °C).

The amplitudes of the filtered time series for SLA, WSC and SST are shown in Fig. 6 a,b,c. The colorbar scales are different from the corresponding scales in Fig. 4 a, b and c to avoid missing information (color contrast) due to regional variability. For SLA, amplitudes up to 10 cm can be found in the Alboran sea, Algerian current area and southeast Crete. Fig. 5a reveals that the filtered (non-annual) amplitudes of the Alboran and Algerian areas represent more than 50% of total local variability. For the area southeast of Crete, less than 10% of the variability is explained. Therefore, the SLA variability in Alboran and Algerian areas is predominately intra-annual (filtered). This is consistent with the observed intra-seasonal formation/disappearance of the Alboran gyres (Vazquez-Cuervo et al., 1996; Heburn and LaViolette, 1990) and the mesoscale activity related with the Algerian current (Millot, 1987; Bouzinac et al., 1998). For WSC, the filtered amplitude contribution has a maximum in the north of the WM, east of the Gulf of Lions and in the North of the Catalan sea (can be related with important episodic wind events in both areas) together with a maximum in the Levantine basin, west of Greece, and southeast of Sicily. The location of the two maxima in the WM coincides with the ones in the annual signal (Fig. 4b). As shown in Fig. 5b, a significant portion is non-annual.

For SST amplitudes of the filtered signal, the spatial distribution is similar to the annual one, but with reduced values. It seems that the latitudinal distribution of temperature variability has an annual period which contributes about 30-40% of the variability (Fig.5c).Thus the non-annual (intra-annual) response is dominant.

b. Canonical correlation analysis of the filtered signal

The next step in the study is the analysis of the filtered signal for SLA, WSC and SST using regular Empirical Orthogonal Functions (EOF) and canonical correlation techniques to evaluate the air-sea coupling for non-seasonal signals. The canonical correlation analysis consists in a decomposition of the data fields for two variables into a set of canonical modes, which are analogous to empirical orthogonal functions (EOFs) for a single field. The canonical correlation analysis gives the covarying patterns and corresponding time series of the two fields. The significance of the modes has to be evaluated afterwards, in the same fashion as it is done with EOFs. For each one of the canonical modes we calculate the fraction of the covariance explained, along with the amplitudes and the spatial patterns for the two variables. This formulation considers that the modes maximize the amount of cross-covariance between the two

fields contained in the lowest modes, compared with maximizing the autocovariance of a single field in EOFs. The first step of the canonical correlation calculation consists in the computation of the EOFs of SLA, WSC and SST. The canonical modes are computed from a full expansion of the EOFs of each variable. The detailed matrix formulation of the canonical correlation analysis can be found in Kelly et al. (1996). EOF modes can be computed ranked by their spatial variance as well as by their temporal variance. Spatial patterns with the strongest horizontal gradients, such as fronts or eddies, should be evident in the dominant modes.

We use the Rule of N (Overland and Preisendorfer, 1982) to select statistically significant EOF modes. The Rule of N is based on considering that the statistically correlated oceanographic/meteorological modes have a percent of variance explained greater than the level of noise. This level of noise is simulated by repeated sampling of principal components computed from a spatially and temporally uncorrelated random process. As Overland and Preisendorfer (1982) pointed out, even if a particular mode fails the Rule of N, this need not eliminate the possibility that other criteria, such as the ability of the particular principal component to closely track the time evolution of a oceanographic/meteorological process in the presence of large noise variance, may still be physically relevant. In our computation we find that only the first EOF mode for SST explains a percent of variability explained greater than the one associated with the noise level. The first six EOF modes for both WSC and SLA also have a percent of variability higher than the level of noise and can a priori be considered statistically significant. Table 2 shows the percent of variability values for the first three EOF modes of SLA, WSC, SST and the level of noise by the Rule of N. Only the first EOF mode of the SST has a percent variability (99.92%) higher than the level of noise for the first mode (4.12%). From the second to the sixth SST modes, the values of the percent of variability for the modes are at least two orders of magnitude lower than the level of noise. For instance, 0.03 and 0.01 are the values for the second and third SST modes respectively, while 2.6% is the level of noise for both the second and the third modes respectively (Table 2). In addition, the correlation required for a 95% level of confidence is calculated to characterize the statistical significance of the canonical modes.

The first phase of the canonical correlation formulation consists in the computation of the EOFs of the SLA, WSC and SST. The fraction of variance in each of the first three EOFs for each variable is shown in Table 2. An FFT was performed on the temporal amplitude to

determine the dominant frequencies and the results are in Table 2. A brief examination of the EOFs will help us to understand the individual trends in the canonical correlation coupled analysis. Following the criteria of the Rule of N, only the first mode is statistically significant for the SST. For the SLA and WSC modes 1 to 6 explain a percent of the variance which is greater than the level of noise. We consider here the first three modes as they explain more than 50% of the variance.

The first EOF mode of SLA explains 47.5% of the variance and the corresponding peaks in the spectra are at 2.1 (semiannual) and 6.3 cycles per year. Modes #2 and 3 are still significant following the Rule of N. The percent of variance explained is 8.9 and 5.2% respectively. Mode #2 has similar spectral content as mode #1. The peaks in the spectra for mode #3 occur at 3.2 and 7.4 cycles per year. As already mentioned, the orbit accuracy of the altimetric data set is of the order of 3 - 5 cm (LeTraon et al., 1995) and the amplitudes of the non-annual SLA signal are of about this same order. In the Appendix, we show that the EOF can extract a signal whose amplitude is near the level of the noise of the data. We generated a synthetic signal which contains an annual signal (10 cm of amplitude), a semiannual signal (3 cm of amplitude), and added noise (5 cm) to test the ability of the method. See the Appendix for more details.

The first mode of WSC explains 55.1% of the variability (10.3 and 8.5 for the second and third respectively) with a number of maxima in the spectra. For the second mode, there is a plateau in the frequency plot (not shown) between 2.1 and 3.2 cycles per year. For both SLA and WSC, the semiannual signal is dominant along with harmonics at 4.2, 3.2, and 6.3 cycles/year. For SST the situation is different. The first EOF mode of the SST contains 99.9% of the variance of the analyzed signal. This first mode is dominant and a steep drop in variance follows for the next modes. The amount of variance explained by the first mode indicates that there is a strong time-varying signal in the data which dominates the temporal variability (Lagerloef and Berstein, 1988). From the spectrum of the temporal amplitude, the dominant signal is 1.05 cycles per year, with a maximum in July (unlike the annual signal with a maximum in October). This near-annual frequency leads the annual signal by about 90 days. These results are consistent with Lagerloef and Bernstein (1988) for a semi-enclosed oceanic basin. We also find two uncoupled annual cycles in the study area. One has its maxima in early summer and the second one in fall. Only the second mode (where the variance is less than the Rule of N noise estimation) is associated with the semiannual frequencies. Modes with small variance are often

disregarded because of their poor statistical significance. Nevertheless, the frequencies from modes #2 and 3 are consistent with the ones obtained for WSC and SLA, as shown in Table 2.

We have computed the canonical correlation modes in pairs for the three variables SLA, WSC and SST. Table 3 shows the relative contribution to the covariance and the correlation of each of the first three canonical modes for SLA/WSC, SLA/SST and SST/WSC.

The SLA/WSC canonical analysis shows that the first three modes contain 78.11, 10.17 and 6.38% of the covariance respectively. The spatial and temporal patterns for the first two modes are shown in Fig. 7 and 8 respectively. The maximum value of the correlation for SLA/WSC is 0.57 for the first mode. Fig. 7a,b shows the spatial pattern of the first mode. The maxima of the WSC spatial pattern coincide locally with zones of maxima of the SLA. These areas are east of Alboran (approximately coincident with the Almeria-Oran front location), east of the Balearic, south Thyrrenian, central Ionian and almost the whole Levantine basin. The locations are partially coincident with areas of maxima in the WSC annual signal, except for the Gulf of Lions and east Alboran areas. For the Balearic, Thyrrenian and Ionian basins, they correspond in location and frequencies to the southeastward winds which are especially intense in the wintertime (Fig. 8a,b, from day 350 to 420 approximately), and follow the path of the eastern part of the Algerian current entering the Strait of Sicily and then continuing downstream as the Ionian current. In addition, local wind changes account for up to 70% of variability of the SLA in the Ionian sea (Larnicol et al., 1995, figure 1). The Levantine sea shows a patchy distribution of maxima for both the first and second modes of SLA. For WSC there is a definite area of positive signature. The overall circulation in the Levantine basin is anticyclonic in October-December and cyclonic in April-June. Circulation patterns show a strong intra-annual and interannual variability. Nevertheless, in the SLA annual map (Fig. 4 a) local maxima are seen in the areas of the Ierapetra and Mersa-Matruh gyres (the latter is off the Egyptian coast), while the canonical spatial patterns of the filtered signal do not give a definitive circulation-like picture in the Levantine sea. This is consistent with model results from Roussenov et al. (1995), who concluded that the Mersa-Matruh gyre has large seasonal cycle strength.

The SLA spatial pattern (Fig. 7b) over the area of the Algerian current and Balearic basin shows a patchy distribution of maxima. These spatial structures can be associated with the anticyclonic mesoscale eddies generated from the Algerian current (merged ERS1-TOPEX/POSEIDON altimetric data provides higher spatial resolution than TOPEX/POSEIDON

data to detect such formations). Most of them are anticyclonic and propagate eastward while attached to the coast. With time, they leave the coast, grow and travel into the interior of the Balearic basin (Millot, 1987).

In the Levantine basin, winds are meridional in summer and mostly zonal in winter. The similarity in the location of areas of maxima for the SLA/WSC first mode is greater in the EM than in the WM which is consistent with the fact that the EM general circulation is more variable than that of the WM and highly forced by winds.

For the area of the Gulf of Lions the maximum appears in the second mode (Fig. 7c) and can correspond to the episodic Mistral wind events. It is known that the Mistral winds blow during the winter (see for example Leaman and Schott, 1991). This fact is consistent with the temporal amplitudes of the SLA/WSC in mode #2, where extremes in both occur during the winter of 1992-93. The east Alboran maxima (associate with the eastern anticyclonic gyre) appear in both the first and second modes for WSC and SLA. This area is known for its strong and variable winds. The SLA maxima in the Algerian current area are not found in the WSC modes. The dominant frequency for this first mode is the semiannual for both SLA and WSC, though secondary peaks occur at 6.2 and 4.2 cycles/year. The second canonical mode of the WSC has a peak at the near-annual frequency of 1.05 cycles per year. Such a frequency is similar to what we found for SST.

As could be anticipated from the EOF analysis, the first mode of the SLA/SST and SST/WSC canonical correlations dominate the covariance. The values are 99.99 and 99.93% respectively. The near-annual response is seen in the frequency spectra of the amplitudes. The first modes of both SLA/SST and SST/WSC have low but significant correlation. Considering the frequencies of the signals involved, low correlations are understandable. The spectra of the second mode of SLA/SST are similar to those of the second mode of SST/WSC. Therefore, for this case, SLA and SST canonical modes show better correlation than for WSC and SST. Although the first mode of SLA/SST has a correlation of 0.34, it displays an anticyclonic eddy-like distribution in the Balearic basin off the Algerian coast and a strong signature associated with the Ierapetra gyre (not shown), in agreement with the SLA/WSC first mode. Besides, for the three first modes of the canonical correlation analysis of the SLA/WSC, SLA/SST and the first mode of SST/WSC, the respective correlations have values which are significant at the 95% level of confidence (see Table 3, values in brackets). The second and third modes of SST/WSC

are not statistically significant.

The values of the correlations we obtain (Table 3) have to be discussed considering also that there are physical processes which may produce SLA and SST fluctuations in the Mediterranean sea with no dynamical link to the WSC, such as the seasonal heating and cooling of the water column causing steric changes in sea level. Numerical models of the Mediterranean sea show the importance of the wind forcing effect on the upper layer (Roussenov et al., 1995; Zavatarelli and Mellor, 1995). However, sensitivity analyses of the models also reveal that other processes are also significant in the upper layer of the Mediterranean and cannot be dismissed, including the flux through the straits and the bottom topography effect. In the Mediterranean sea, evaporation exceeds total precipitation and river runoff. The resulting water deficit is compensated by the inflow of Atlantic water (which also has fluctuations) through the strait of Gibraltar. The Atlantic water becomes more saline in its eastward migration and is renamed as Modified Atlantic Water. It enters the EM through the strait of Sicily. The interaction of the processes which produce time fluctuations in the upper layer and more stationary ones (such as bottom topography) contributes to the dynamical variability at basin and subbasin scale (Alvarez et al., 1994).

c. Linear barotropic vorticity equation

To determine the importance of the barotropic response in the Mediterranean sea, the barotropic vorticity equation will be computed. In the quasi-geostrophic limit the dynamics of the ocean's response can be described to a large extent by the linear barotropic vorticity equation (Fu and Davidson, 1995):

$$\frac{\partial}{\partial t}\nabla^2\eta + \beta\frac{\partial\eta}{\partial x} - \frac{f}{H}\left[\frac{\partial\eta}{\partial x}\frac{\partial H}{\partial y} - \frac{\partial\eta}{\partial y}\frac{\partial H}{\partial x}\right] = \frac{f}{\rho g}\left[\text{curl}\left(\tau/H\right)\right]_z \qquad (2)$$

where η is the sea level, H is the ocean depth, ρ is the water density, τ is the wind stress, f is the Coriolis parameter and β is the latitudinal variation of the Coriolis parameter (Apel, 1987). The first term of the left-hand side of (2) is the time rate of change of the relative vorticity, the second term is the advection of the planetary vorticity and the third term is the advection of the vorticity induced by the bottom topography. The right-hand side of (2) is the forcing produced

by the wind stress curl. As we have already described, wind stress and sea level are available in the present study and can be used to compute (2) on the same time/space grid context as that used for the canonical correlation calculations. The annual harmonic was removed from both data sets. Two additional data sets are necessary to compute (2). The first one is the bathymetry data, which was extracted from the ETOPO5 global elevation database (with a resolution of 12 points per degree). The second one is the seasonal water density fields, which were retrieved from the climatologies available at the Mediterranean Oceanographic Data Base (MODB) with an initial resolution of 0.2 degrees. These data sets were interpolated to the above mentioned spatial grid. We have applied the canonical correlation technique to both sides of equation (2) in order to obtain an estimate of the regions where the wind forcing has sufficient energy to account for the barotropic vorticity variation.

The correlation between the results of the left- and right-hand side of equation (2) is low (0.32). The results of the application of the canonical correlation technique to both sides of equation (2) display an analogous behavior. The first canonical mode only accounts for 37% of the relative contribution to the covariance and the correlation is 0.29 (with 0.26 as the correlation required for the 95% level of confidence). We can see the first canonical mode for the left-hand side (labeled Baroleft) in Fig. 9a and that corresponding to the right-hand side (labeled Baroright) in Fig. 9b. From the second mode to higher modes, the correlation is lower than that the required for the 95% of confidence. For instance, mode #2 (Fig. 9 c and d) has a relative covariance of 29.9%, a correlation of 0.14 and the one for the 95% level of confidence is 0.31. Thus, only the first mode can be considered statistically significant. The temporal amplitudes for the first and second modes display low correlation. The FFT analysis of the temporal amplitudes for the first mode gives 2.1,3.5 and 4.2 cycles per year as the most important frequencies for the wind stress, while the result is 2.2, 3.9 and 6.1 for the sea level. The correlation is high only in specific areas of the Adriatic sea, by the strait of Sicily and off-shore of Egypt. These areas, especially for the Strait of Sicily, are characterized by strong wind forcing (as we have seen in Fig. 4b and 7a). The Strait of Sicily coincides with an area known to be dominated by topographic Rossby waves and because it is a narrow strait, the barotropic signal is amplified (Pierini, 1996). In addition, from Pierini (1996) such modes are excited in the winter and autumn months, consistent with results from Fig. 10a and b.

4. Summary and conclusions

The objective of this study was to evaluate the coupling between the ocean and the atmosphere to assess the potential role of WSC and/or SST space/time variations as forcing mechanisms of the SLA variability in the Mediterranean sub-basins from 440 days of the three simultaneous satellite data sets. Despite the short time period, our analysis yields some significant modes of coupling. The data sets have been analyzed in the light of its frequency components.

The annual signal of SLA is dominant in both the EM and WM and it explains more than 70% of the SLA variability for most of the Mediterranean sea (with significant exceptions in the Alboran and Algerian areas). The SLA annual regional pattern has a significant correlation with the WSC one, especially in the areas where several maxima are observed. These specific correlated maxima are located where the percent variability explained by the WSC annual signal is the highest in the Mediterranean (in the Ionian and Levantine seas). Consequently, for the annual frequency, WSC is a statistically significant forcing candidate of SLA in those areas where most of the SLA and WSC of the variability is precisely annual.

The SST annual signal explains only 30-40% of the total SST variability and is dominated by the more intense annual warming of the EM compared with the WM. The spatial distribution of the SST annual map is almost horizontal or latitudinal, due to large-scale annual warming and cooling (minima in spring and maxima in fall). In an annual sense, the EM reaches higher surface temperatures later than the WM. This can be due to a latitude effect, as the EM is located more southerly than the WM and to the cool Atlantic inflow into the WM through the Gibraltar strait. Not only for the SST annual signal, but also for the WSC and SLA ones, the range of variation of the values reached is wider for the EM than for the WM. SST and SLA annual signals are in phase in the Mediterranean sea. In addition, no apparent spatial correlation can be made with the SST annual map and the corresponding SLA and WSC maps.

The EOF analysis of the filtered SST (annual signal removed) shows that the the first mode dominates any other temporal signal and explains 99.9% of the variability. A near-annual frequency of 1.05 cycles per years is responsible for this large variance. It is uncoupled with the SST annual signal: the near-annual maximum precedes the seasonal signal by about 90 days, having its maximum in July (unlike the annual signal in October). This behavior is consistent in phase with the results of Lagerloef and Bernstein (1988) in the semi-enclosed coastal basin of

the Santa Barbara Channel. The near-annual frequency of 1.05 cycles per year also is seen in the WSC second canonical mode as non-dominant.

Coupling at the semiannual period can be found between the SLA and the WSC for the first canonical mode. This mode explains 78% of the covariance and has a spatial correlation of 0.57. The maxima of the WSC spatial pattern coincides locally with zones of maxima seen in the SLA. These areas are east of the Alboran (approximately coincident with the Almeria-Oran front location), east of the Balearic, south Thyrrenian, central Ionian and almost the whole Levantine basin. The SLA spatial pattern (Fig. 7b) over the area of the Algerian current and Balearic basin shows a patchy distribution of maxima. These spatial structures can be associated with the anticyclonic mesoscale eddies generated from the Algerian current. The Levantine sea shows a patchy distribution of maxima for both the first and second modes of SLA. In the SLA annual map (Fig. 4a) local maxima coincide in location with the usual position of the Ierapetra and Mersa-Matruh gyres (the latter is off the Egyptian coast), while the canonical spatial patterns of the filtered signal do not give a definitive circulation-like picture in the Levantine sea. Although the SLA/SST first mode has a correlation of 0.34, it also displays an anticyclonic eddy-like distribution in the Balearic basin off the Algerian coast and a strong signature associated with the Ierapetra gyre (plot not shown), in agreement with the SLA/WSC first mode.

It is believed (Fu and Davidson, 1995) that sea level variations at the seasonal and interannual timescales are dominated by the ocean's baroclinic fluctuations, while the barotropic variability is expected at shorter time scales. The calculation of the canonical modes of both sides of equation (2) shows that the response of the Mediterranean sea to the wind forcing cannot be fully described by the barotropic vorticity equation given by (2). In only a few areas the local barotropic response is dominant, such the Strait of Sicily and part of the Adriatic and Catalan sea.

The time frame of 440 days does not allow us to evaluate interannual variability. Longer data sets would be necessary to study such variations. This would imply merging the TOPEX/POSEIDON with the ERS2 data to create a product with the same resolution as the sea level gridded data used in this study. Evaluation of the percent of variability between WSC/SLA and SST/SLA is difficult and our results are only statistical estimations. In addition, no conclusions about the phase of the variables have been reached.

From the results of this study we conclude that to fully understand the physics of the circulation in the Mediterranean sea and the action of the forcing mechanisms the statistical analysis should be compared with regional circulation models and data assimilation techniques applied on the Mediterranean sea.

Appendix: EOF analysis for a signal + noise synthetic data set

Estimates of the error in the merged ERS1-TOPEX/POSEIDON altimetric data set indicate an accuracy of 3-5 cm (LeTraon et al., 1995). Thus the semiannual period, with an amplitude of approximately the same order, is near the noise level of the data. A simulation was run to determine whether the EOF technique can extract a signal whose amplitude is near the level of noise of the data.

Synthetic values of the SLA were produced at the same time-space grid as the merged altimetric data set. Three sets of waves were generated: two with an amplitude of 10 cm at the annual period and associated with two different wavelengths; the third wave with an amplitude of 3 cm at the semiannual period. A Gaussian random noise with a standard deviation of 5 cm was added to the waves. Figure 11 shows the temporal amplitudes of the first three EOF modes from the waves+noise data set, as well as the amplitudes for the first two EOF modes from the case with only the noise. The amplitudes of the three EOF modes from the waves+noise data set show respectively: the two annual signals (with difference in phase associated with the different wavelengths) and the semiannual one. The percent of variance of the two annual modes is 31 and 27% respectively. The semiannual mode has 5% of the variance. The amplitude of the extracted semiannual signal is 2.8 cm. The maximum amplitude of the two first EOF modes from the pure noise case is approximately 2 cm and no periodicity is evident. The correspondent percent of variability is 3% for both modes.

This simulation shows that the EOF technique constitute a powerful tool for extracting periodic signal from a noisy data set, even when the amplitude of the periodic signal is of the same magnitude of the noise. Thus, the semiannual mode cannot be dismissed a priori as noise.

Acknowledgments. The authors thank Wenqing Tang and W.Timothy Liu (both at JPL/Caltech) for providing the ERS1 scatterometer wind velocities and wind-related software. The merged ERS1- TOPEX/POSEIDON data set was kindly provided by Pierre-Yves LeTraon (CLS, Toulouse, France) and Nadia Ayoub (CNRS/CNES, Toulouse, France). The NOAA/NASA AVHRR Pathfinder project provided the sea surface temperature data via JPL-PODAAC. E.G.-G. is financially supported by the *Ministerio de Educacion y Cultura* (Spain) within 'Plan de Formacion de Doctores y Tecnologos en el Extranjero' by way of a Postdoctoral Fellowship at JPL/Caltech. J.V.-C. is currently under contract with NASA. We also thank M.-E. Carr, P. Cornillon, M. Gacic, and two anonimous reviewers for their comments.

References

ALVAREZ, A., TINTORE, J., HOLLOWAY, G., EBY, M. and BECKERS, J.M., 1994, Effect of topographic stress on circulation in the western Mediterranean. Journal of Geophysical Research, 99 (8), 16053-16064.

APEL, J.R., 1987, Principles of Ocean Physics. London. Academic Press, 634 pp.

BOUZINAC, C., MILLOT C., VAZQUEZ J. and FONT J., 1998, Complex Empirical Orthogonal Functions analysis of ERS1 and TOPEX/POSEIDON combined altimetric data in the region of the Algerian Current. Journal of Geophysical Research, 103 (4), 8059-8071.

FONT, J., 1987, The path of the Levantine Intermediate Water to the Alboran Sea. Deep-Sea Research, 34 (10), 1745-1755.

FU, L.L and DAVIDSON R., 1995, A note on the barotropic response of sea level to time-dependent wind forcing. Journal of Geophysical Research, 100 (12), 24955-24963.

GACIC, M., MARULLO S., SANTOLERI R. and BERGAMASCO A., 1997, Analysis of the seasonal and interannual variability of the sea surface temperature field in the Adriatic Sea from AVHRR data (1984-1992). Journal of Geophysical Research, 102 (10), 22937-22946.

GILL, A. E., NIILER, P.P., 1973, The theory of the seasonal variability in the ocean. Deep-Sea Research, 20, 141-177.

HEBURN, G.W. and LAVIOLETTE P.E., 1990, Variations of the anticlyclonic gyres found in the Alboran Sea. Journal of Geophysical Research, 95, 1599-1614.

KELLY, K.A., CARUSO M.J. and SINGH S., 1996, Observations of atmosphere-ocean coupling in the midlatitude western boundary currents. Journal of Geophysical Research. 101 (3), 6295-6312.

LARNICOL G., LE TRAON P.Y, AYOUB N. and DEMEY P., 1995, Mean sea level and surface circulation of the Mediterranean from 2 years of TOPEX/POSEIDON altimetry. Journal of Geophysical Research. 100 (12), 25163-25178.

LAGERLOEF, G.S. and BERNSTEIN R.L., 1988, Empirical Orthogonal Function analysis of AVHRR surface temperature patterns in Santa Barbara Channel. Journal of Geophysical Research, 93 (6) 6863-6873.

LEAMAN, K.D. and SCHOTT F.A., 1991, Hydrographic structure of the convection regime in the Gulf of Lions: winter 1987. Journal of Physical Oceanography, 21, 575-598.

LE TRAON, P.Y., GASPAR P., BOUYSSEL F. and MAKHMARA H., 1995, Using Topex Poseidon data to enhance ERS1 data. Journal of Atmospheric and Oceanic Technology, 12 (1), 161-170.

MALANOTTE-RIZZOLI, P. and BERGAMASCO A., 1989, The circulation of the eastern Mediterranean. Part I: the barotropic wind-driven circulation. Oceanologica Acta, 12, 335-351.

MALANOTTE-RIZZOLI, P. and BERGAMASCO A., 1991, The wind and thermally driven circulation of the eastern Mediterranean Sea. Part II: the baroclinic case. Dynamics of Atmospheres and Oceans, 15, 355-419.

MILLOT, C., 1987, Circulation in the Western Mediterranean Sea. Oceanologica Acta, 10 (2), 143-149.

OVERLAND, J.E. and PREISENDORFER R.W., 1982, A significance test for principal components applied to a cyclone climatology. Monthly Weather Review, 110 (1), 1-4.

PIERINI, S., 1996, Topographic Rossby modes in the Strait of Sicily. Journal of Geophysical Research, 101 (3), 6429-6440.

ROUSSENOV, V., STANEV E., ARTALE V. and PINARDI N., 1995, A seasonal model of the Mediterranean sea general circulation. Journal of Geophysical Research, 100, 13515-13538.

SMITH, S.D., 1980, Wind stress and heat flux over the ocean in gale force winds. Journal of Physical Oceanography, 10, 709-726.

VAZQUEZ-CUERVO, J., FONT J. and MARTINEZ-BENJAMIN J.J., 1996, Observations on the circulation in the Alboran Sea using ERS1 altimetry and sea-surface temperature data. Journal of Physical Oceanography, 26 (8), 1426-1439.

WUNSCH, C., 1972, Bermuda sea level in relation to tides, weather, and baroclinic fluctuations. Reviews of Geophysics, 10, 1-49.

ZAVATARELLI, M. and MELLOR G.L., 1995, A numerical study of the Mediterranean Sea circulation. Journal of Physical Oceanography, 25 (6), 1384-1414.

Tables

Table 1: SLA, WSC and SST ranges reached in the WM and EM with the mean values removed.

	SLA (cm)	WSC (10^{-9}dyn/cm^3)	SST(°C)
WM	(-8.1,8.1)	(-1.6,1,6)	(-7.5,7.5)
EM	(-9.4,9.4)	(-2.2,2.2)	(-8.9,8.9)

Table 2: Percent of variance in each of the first three EOFs for SLA, WSC, SST and rule of N. Frequencies via FFT of the temporal amplitudes.

	Variance % in mode #:			Main frequencies (cycles/year) in mode #:		
Variable	1	2	3	1	2	3
SLA	47.5	8.9	5.2	2.1, 6.3	2.1, 3.2, 6.3	7.4,10.5
WSC	55.1	10.3	8.5	2.1, 4.2, 6.3	[2.1, 3.2], 7.4	2.1, 3.2, 8.4
SST	99.9	0.03*	0.01*	1.05	2.1, 4.2, 10.5	3.2, 5.2, 9.5
Rule of N	4.1	2.6	2.6			

**Smaller variance than the rule of N estimations*

Table 3: Relative contribution to the covariance and correlation of each of the first three Canonical modes for SLA/WSC, SLA/SST and SST/WSC. In brackets, correlation required for a 95% level of confidence. Frequencies via FFT of the temporal amplitudes.

	Covariance % mode #:			Correlation mode#:		
Variable	1	2	3	1	2	3
SLA/WSC	78.11	10.17	6.38	0.57(0.31)	0.14(0.07)	0.33(0.21)
SLA/SST	100.00	0.00	0.00	0.34(0.22)	0.53(0.17)	0.47(0.27)
SST/WSC	99.93	0.04	0.02	0.66(0.49)	0.10(0.19)	0.54(0.34)

	Main frequencies (cycles/year) in mode #:		
Variable	1	2	3
SLA/WSC	2.1,6.3 / 2.1, 4.2	2.1,3.2,6.3 / 1.05,4.2,7.4	2.1, 7.4 / 3.2, 4.2
SLA/SST	2.1,6.3 / 1.05	2.1,6.3,7.4 / 2.1, 4.2,5.2	3.2, 5.2 / [3.2,5.3],9.5
SST/WSC	1.05 / 2.1, 4.2	2.1,3.2,5.2 / 2.1,4.2,7.4	2.1, 4.2 / 2.1,3.2

Figure Captions

1. (a) Main sub-basins of the Mediterranean Sea. The dashed-line rectangle locates schematically the Algerian current, which flows eastward alongshore the Mediterranean coast of Africa within 0- 11°E and 36- 38°N approximately and enters the Strait of Sicily).
   (b) Ground track locations over the Mediterranean Sea for the TOPEX/POSEIDON orbits (thick lines) and for the ERS1 orbit in 35 day repeat (thin lines).

2. (a) Spatially averaged power spectral density (PSD hereafter) of the sea level anomaly over the Mediterranean Sea observed in the period from October 92 to December 93.
   (b) Spatially averaged PSD of the sea surface temperature over the Mediterranean Sea.
   (c) Spatially averaged PSD of the wind stress curl over the Mediterranean Sea.

3. (a) Basin-wide spatial average of the annual signal for the sea level anomaly in centimeters. Dashed lines are the spatial averages for the Eastern Mediterranean basin while solid lines are the spatial averages for the Western Mediterranean basin.
   (b) Same as (a) except for the wind stress curl in dynes/cm^3.
   (c) Same as (a) except for the sea surface temperature in degrees Celsius.

4. Amplitude of annual cycle of (a) the sea level in centimeters, (b) the wind stress curl in 10^{-10} dynes/cm^3 and (c) the sea surface temperature in degrees Celsius.

5. Percent variability explained by annual cycle fit of (a) the sea level, (b) the wind stress curl and (c) the sea surface temperature.

6. Amplitude of non-annual signal of (a) the sea level in centimeters, (b) the wind stress curl in 10^{-10} dynes/cm^3 and (c) the sea surface temperature in degrees Celsius.

7. (a) Spatial pattern of the first canonical mode of the wind stress curl
   (b)Same as (a) except for the sea level anomaly.

(c) Spatial pattern of the second canonical mode of the wind stress curl.

(d) Same as (c) except for the sea level anomaly.

8. (a) Temporal amplitude of the first canonical mode of the wind stress curl (solid line) and sea level anomaly (dashed line).

(b) Same as (a) except for the second canonical mode.

9. (a) Spatial pattern of the first canonical mode of the left-hand side terms of the linear barotropic vorticity equation

(b) Same as (a) except for the right-hand side terms of this equation.

(c) Spatial pattern of the second canonical mode of the linear barotropic vorticity equation

(d) Same as (c) except for the right-hand side terms of this equation.

10. (a) Temporal amplitude of the first canonical mode of the left-hand side terms of the linear barotropic vorticity equation (solid line) and the right-hand side terms (dashed line).

(b) Same as (a) except for the second canonical mode.

11 Temporal amplitude (cm) of the EOF modes generated from synthetic data considering:

- Waves+noise case: the two annual signals correspond to the first (solid line) and second (dashed line) modes; the semiannual signal correspond to the third.
- Pure noise case: amplitudes of the first (diamonds) and second (triangles) modes.

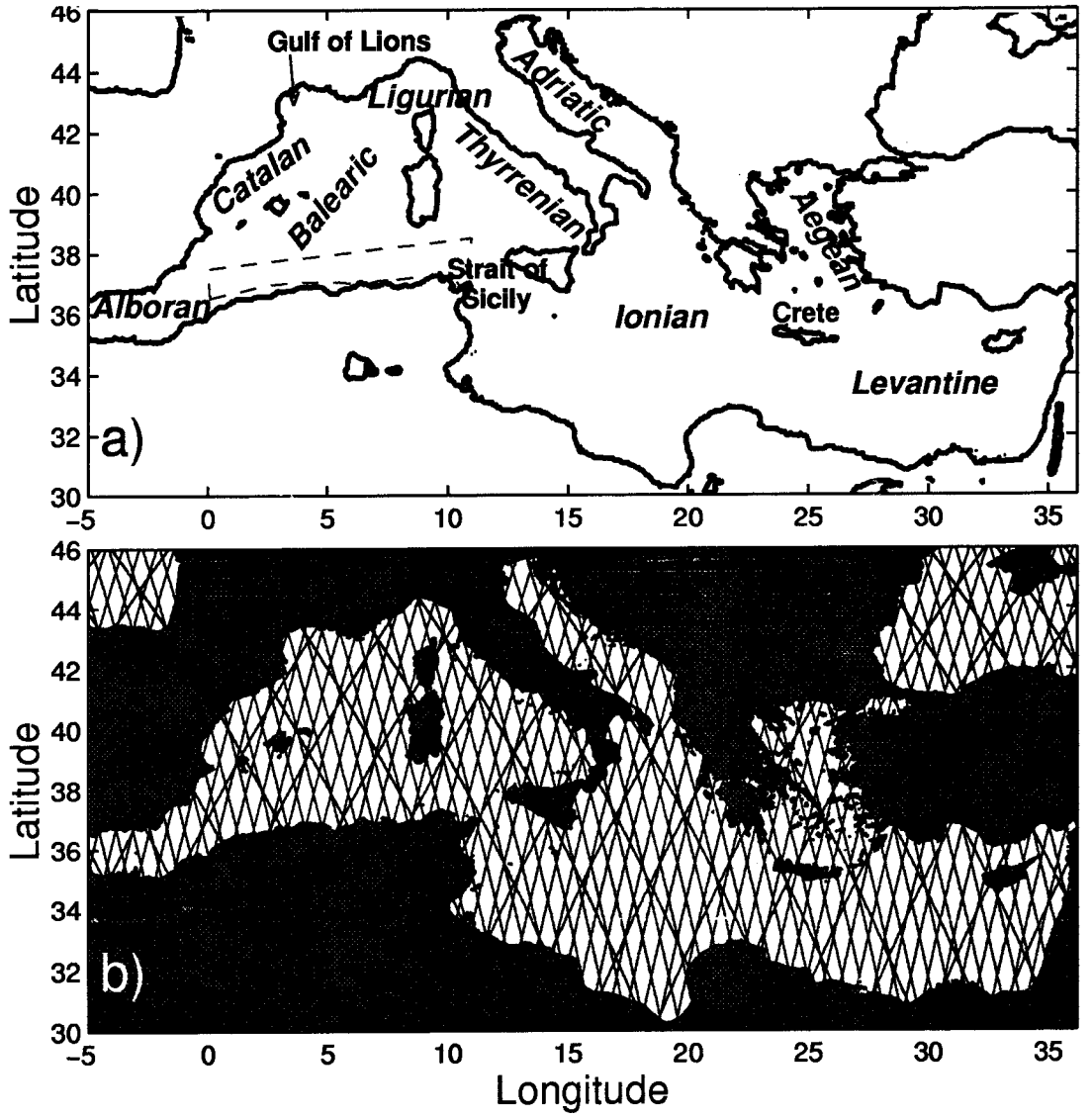
Gulf of Lions
Ligurian
Adriatic
Catalan
Balearic
Thyrrenian
Aegean
Alboran
Strait of Sicily
Ionian
Crete
Levantine
a)
b)
Latitude
Longitude
46
44
42
40
38
36
34
32
30
-5
0
5
10
15
20
25
30
35

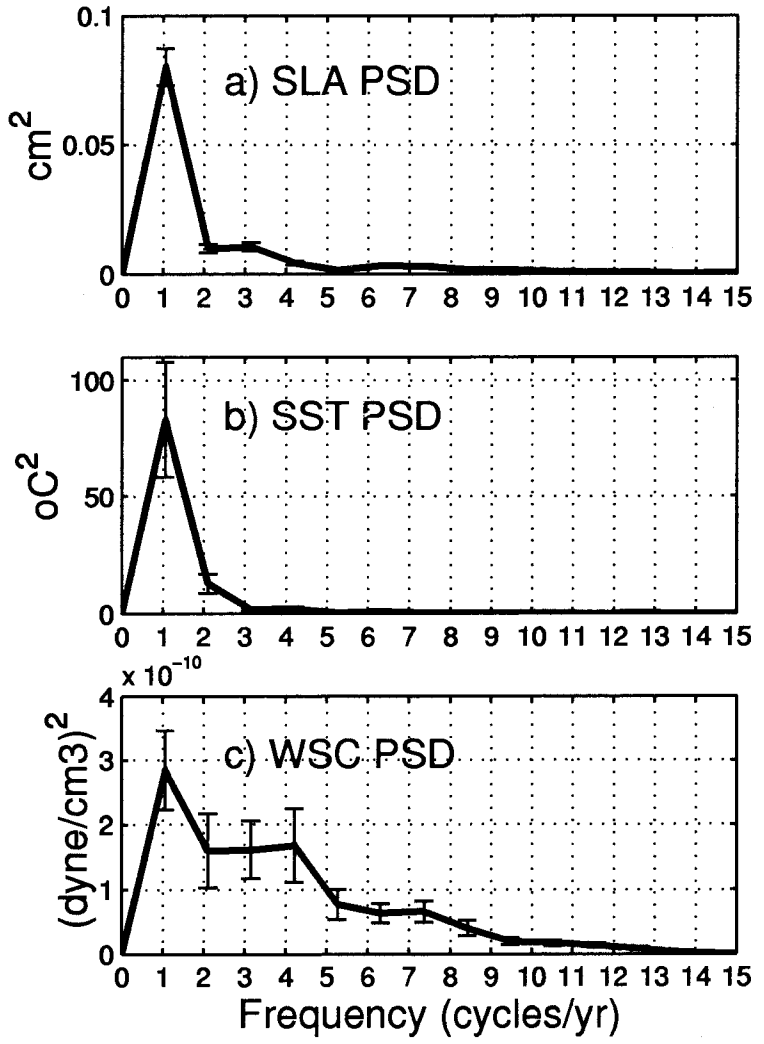
a) SLA PSD
cm2
0.1
0.05
0
0 1 2 3 4 5 6 7 8 9 10 11 12 13 14 15
b) SST PSD
oC2
100
50
0
0 1 2 3 4 5 6 7 8 9 10 11 12 13 14 15
x 10−10
c) WSC PSD
(dyne/cm3)2
4
3
2
1
0
0 1 2 3 4 5 6 7 8 9 10 11 12 13 14 15
Frequency (cycles/yr)

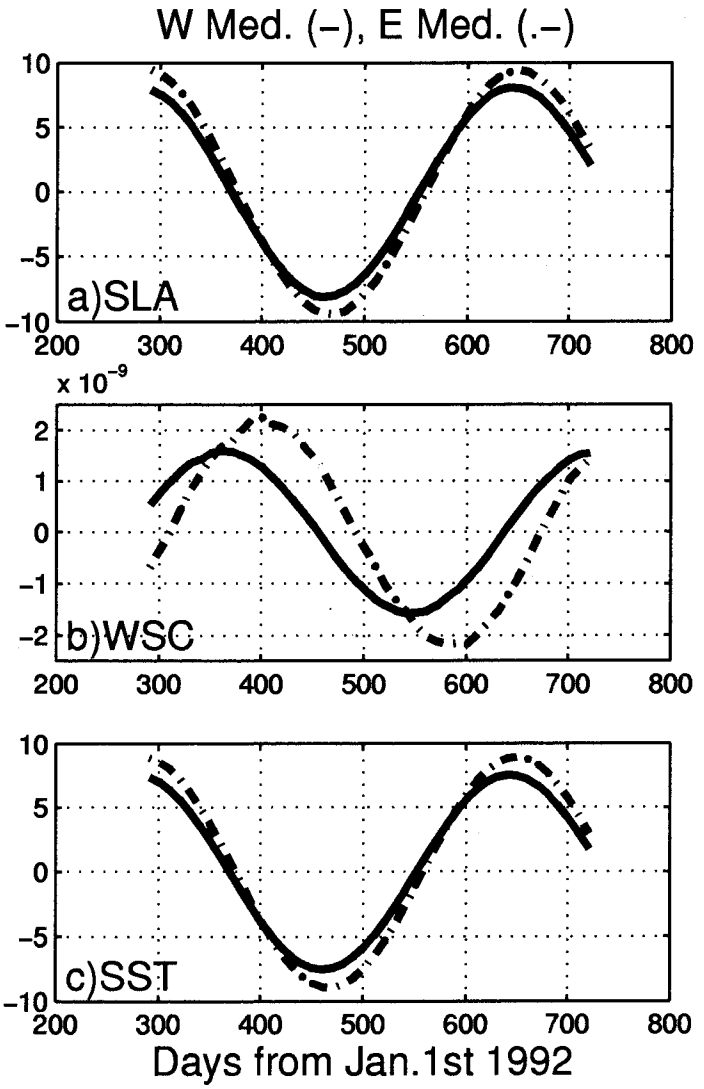
W Med. (–), E Med. (.–)
10
5
0
-5
-10
a)SLA
200
300
400
500
600
700
800
x 10^-9
2
1
0
-1
-2
b)WSC
200
300
400
500
600
700
800
10
5
0
-5
-10
c)SST
200
300
400
500
600
700
800
Days from Jan.1st 1992

SLA amplitude of annual signal

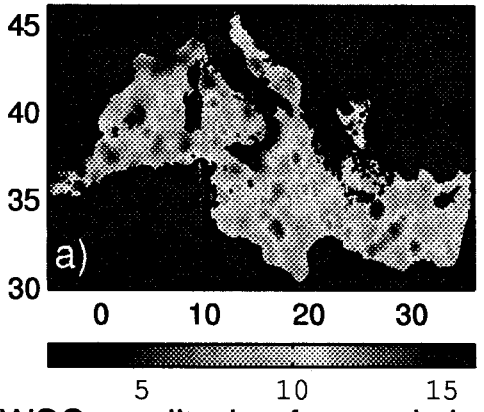

WSC amplitude of annual signal

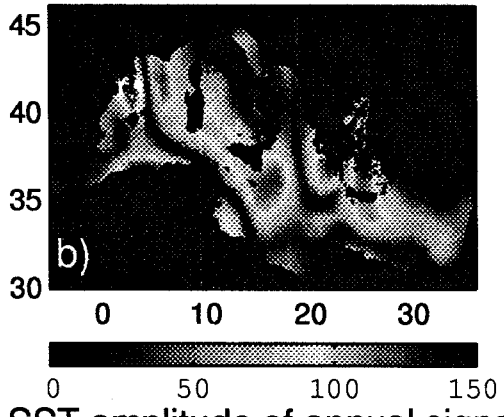

SST amplitude of annual signal

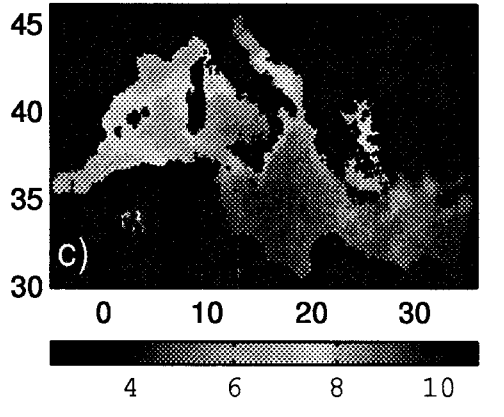

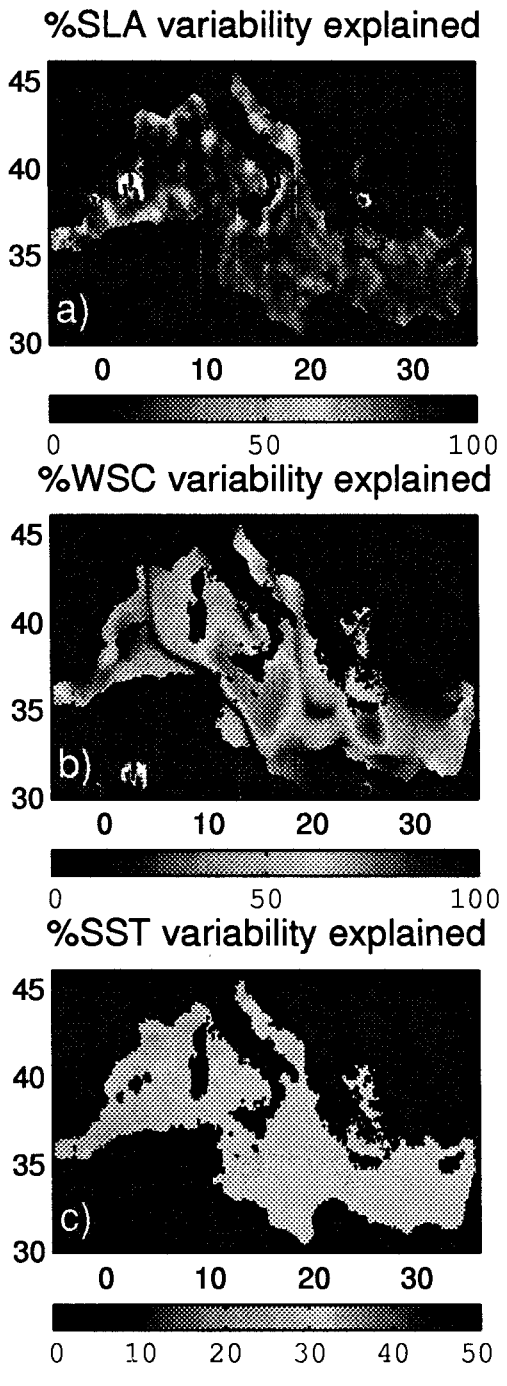
%SLA variability explained
45
40
35
30
a)
0
10
20
30
0
50
100
%WSC variability explained
45
40
35
30
b)
0
10
20
30
0
50
100
%SST variability explained
45
40
35
30
c)
0
10
20
30
0
10
20
30
40
50

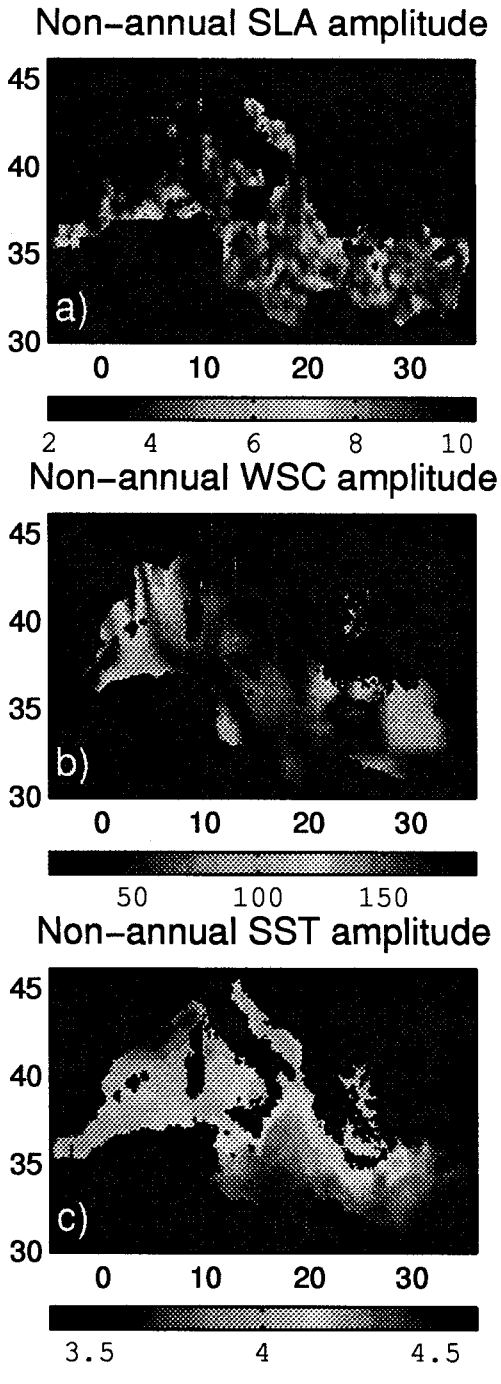
Non-annual SLA amplitude
45
40
35
30
a)
0
10
20
30
2
4
6
8
10
Non-annual WSC amplitude
45
40
35
30
b)
0
10
20
30
50
100
150
Non-annual SST amplitude
45
40
35
30
c)
0
10
20
30
3.5
4
4.5

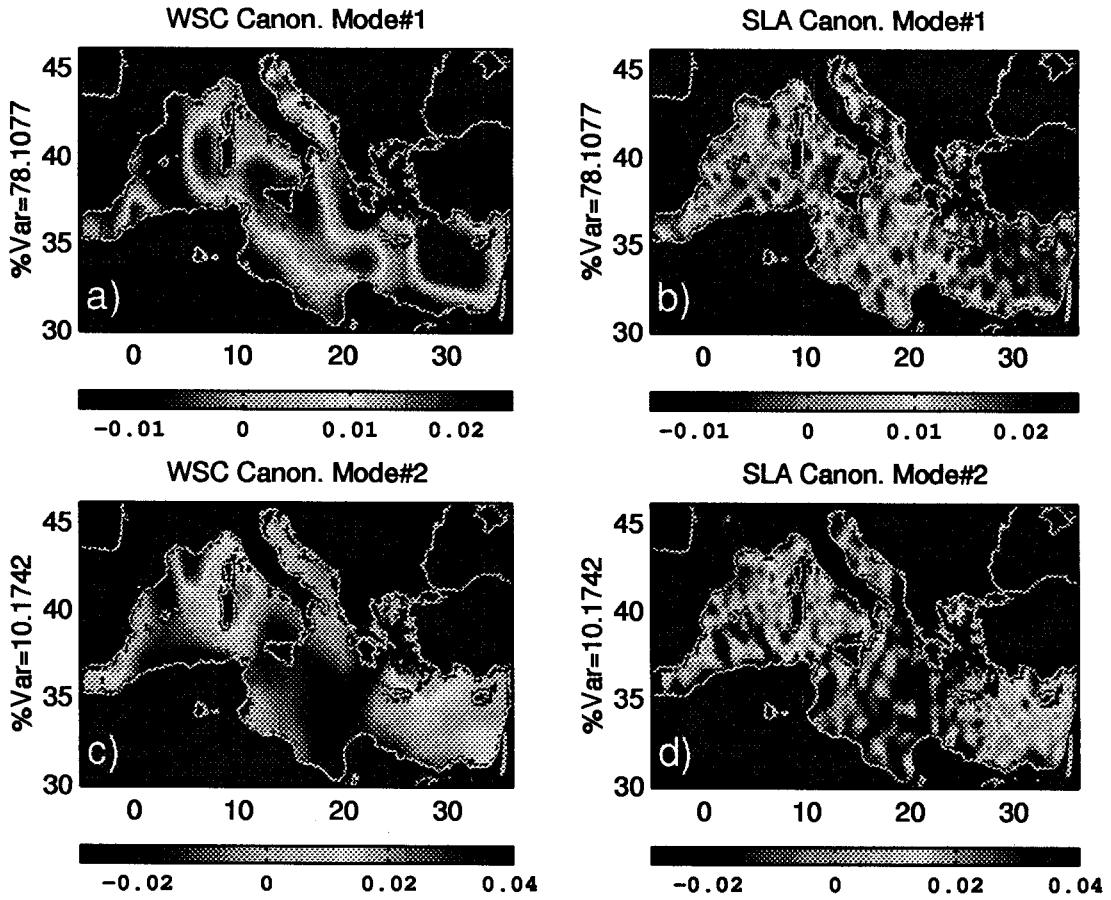
WSC Canon. Mode#1
SLA Canon. Mode#1
WSC Canon. Mode#2
SLA Canon. Mode#2
%Var=78.1077
%Var=10.1742
a)
b)
c)
d)
45
40
35
30
0
10
20
30
-0.01
0
0.01
0.02
-0.02
0.04

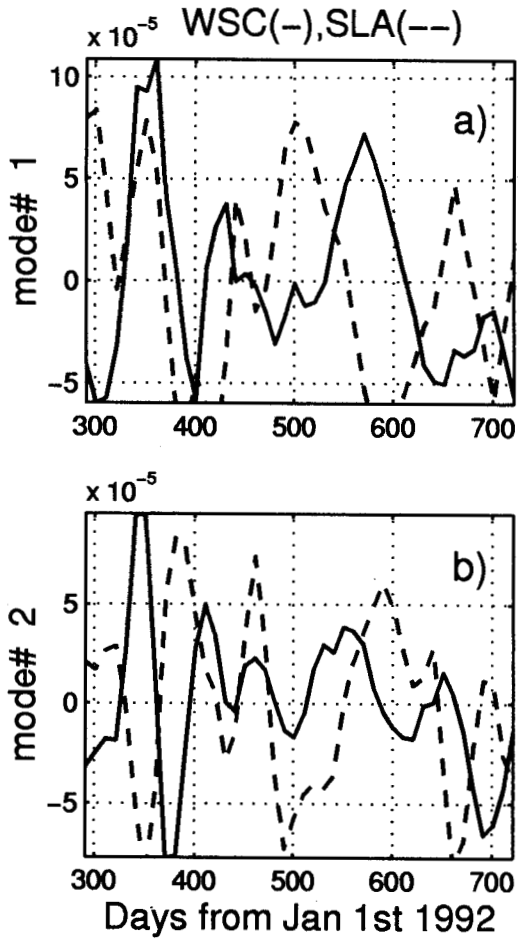
WSC(−),SLA(−−)
x 10^-5
mode# 1
a)
10
5
0
−5
300
400
500
600
700
x 10^-5
mode# 2
b)
5
0
−5
300
400
500
600
700
Days from Jan 1st 1992

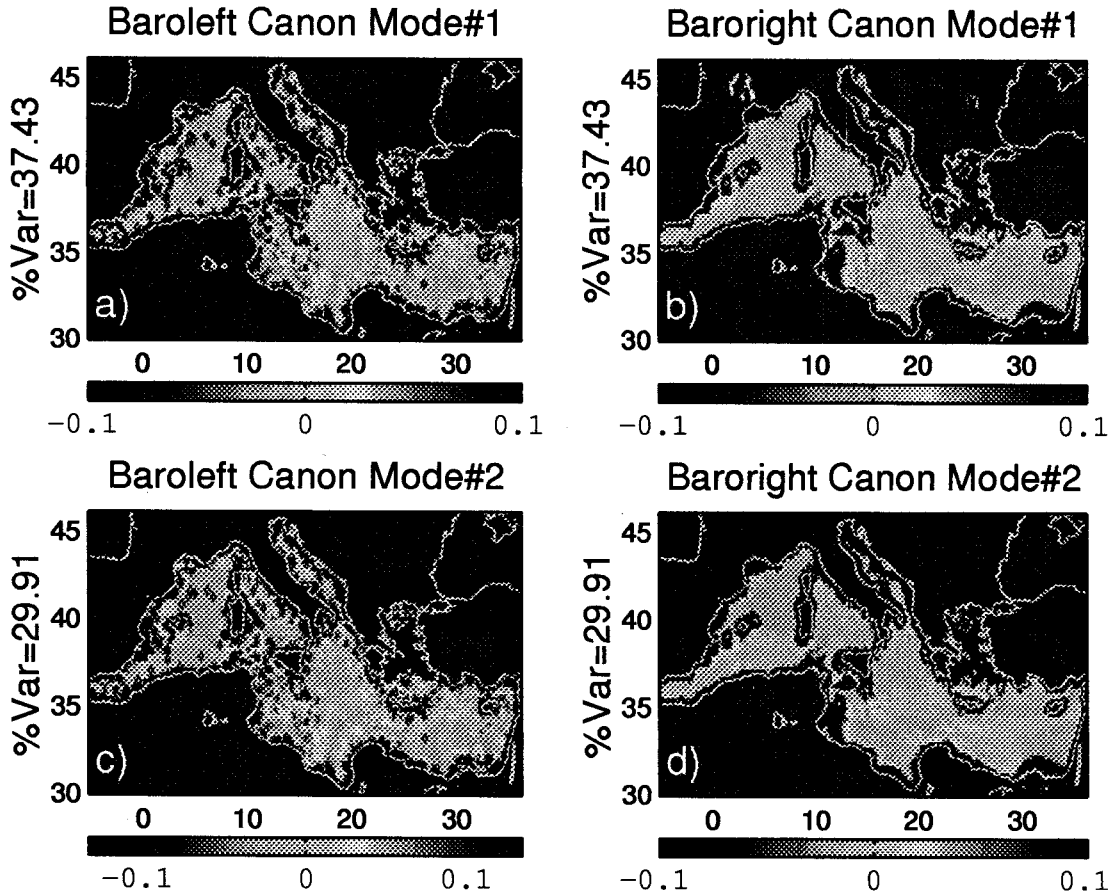
Baroleft Canon Mode#1
%Var=37.43
45
40
35
30
a)
0
10
20
30
−0.1
0
0.1
Baroright Canon Mode#1
%Var=37.43
45
40
35
30
b)
0
10
20
30
−0.1
0
0.1
Baroleft Canon Mode#2
%Var=29.91
45
40
35
30
c)
0
10
20
30
−0.1
0
0.1
Baroright Canon Mode#2
%Var=29.91
45
40
35
30
d)
0
10
20
30
−0.1
0
0.1

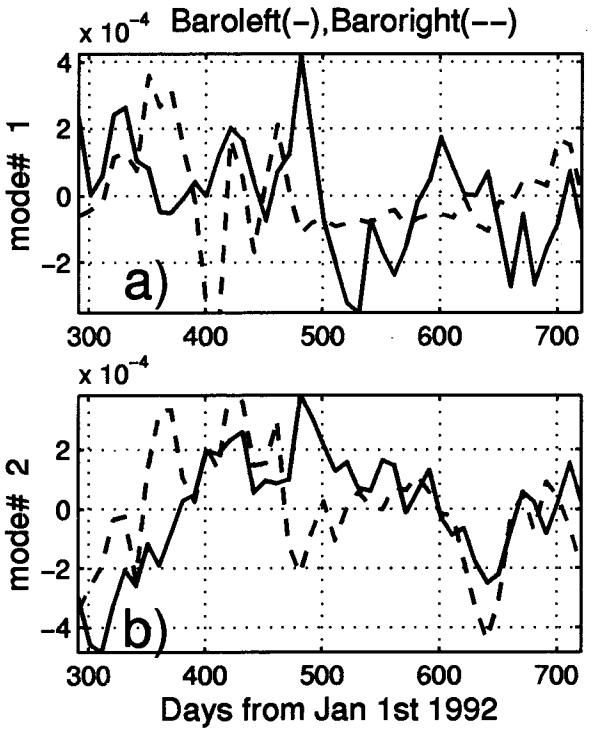
x 10^-4 Baroleft(-),Baroright(--)
mode# 1
4
2
0
-2
a)
300
400
500
600
700
x 10^-4
mode# 2
2
0
-2
-4
b)
300
400
500
600
700
Days from Jan 1st 1992

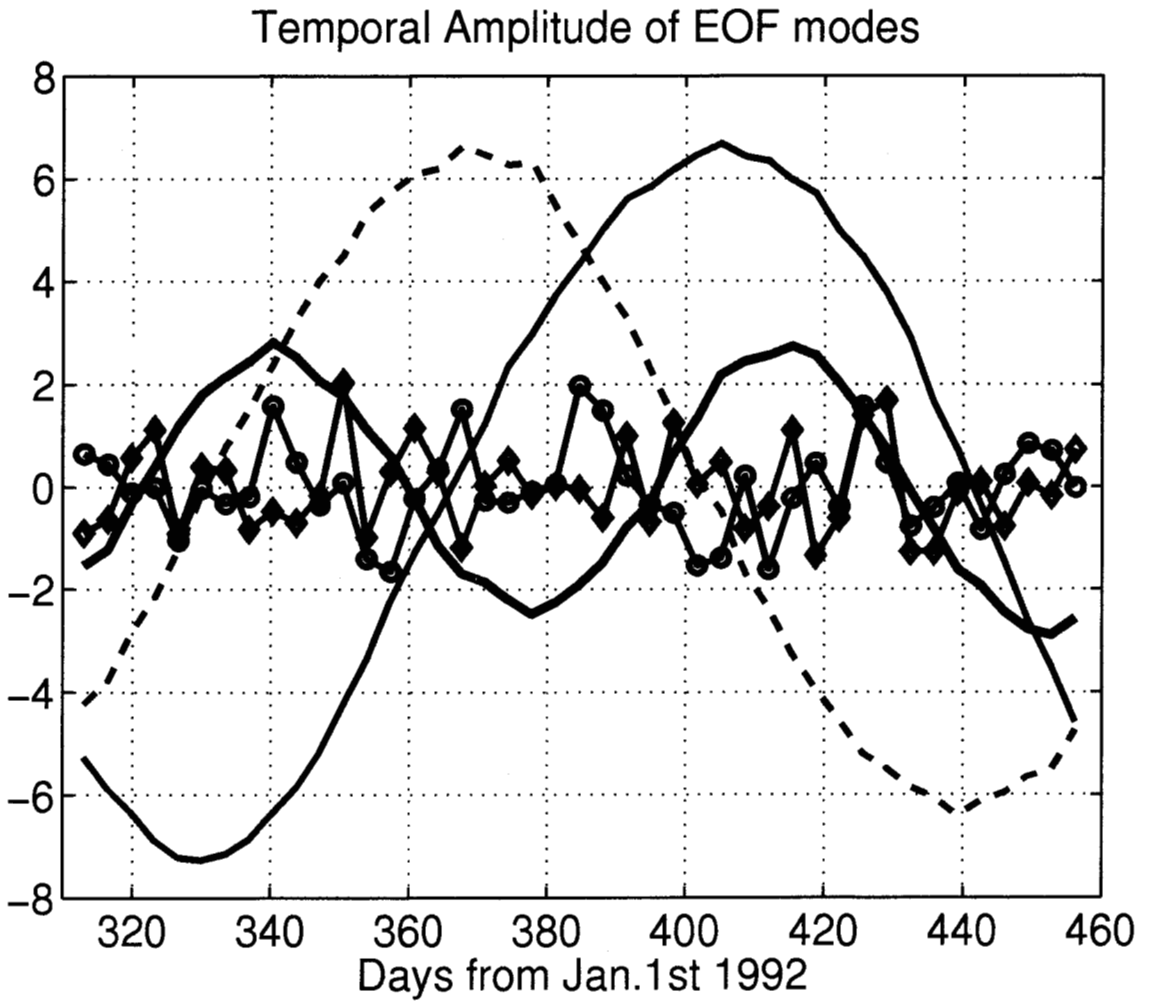
Temporal Amplitude of EOF modes
8
6
4
2
0
−2
−4
−6
−8
320
340
360
380
400
420
440
460
Days from Jan.1st 1992